Chemical Science

Accepted Manuscript

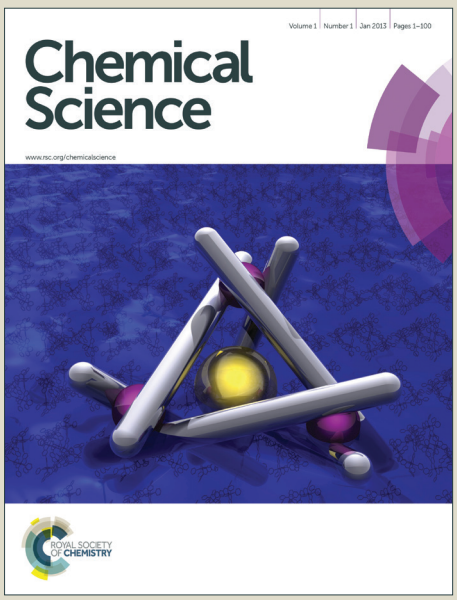

ROYAL SOCIETY OF CHEMISTRY

www.rsc.org/chemicalscience

Journal Name

RSCPublishing

ARTICLE

Jahn-Teller orbital glass state in the expanded fcc Cs_3C_{60} fulleride

Cite this: DOI: 10.1039/xoxxoooooox

A. Potočnik,[a] A. Y. Ganin,[b] Y. Takabayashi,[c] M. T. McDonald,[c] I. Heinmaa,[d] P. Jeglič,[a,e] R. Stern,[d] M. J. Rosseinsky,[b] K. Prassides[c,f] and D. Arčon[a,g]

Received ooth March 2014,
Accepted ooth March 2014

DOI: 10.1039/xoxxoooooox

www.rsc.org/

The most expanded fcc-structured alkali fulleride, Cs_3C_{60} is a Mott insulator at ambient pressure because of the weak overlap between the frontier t_{1u} molecular orbitals of the C_{60}^{3-} anions. It has a severely disordered antiferromagnetic ground state that becomes a superconductor with a high critical temperature, T_c of 35 K upon compression. The effect of the localised t_{1u}^3 electronic configuration on the properties of the material is not well-understood. Here we study the relationship between the intrinsic crystallographic C_{60}^{3-} orientational disorder and the molecular Jahn-Teller (JT) effect dynamics in the Mott insulating state. The high-resolution ^{13}C magic-angle-spinning (MAS) NMR spectrum at room temperature comprises three peaks in the intensity ratio 1:2:2 consistent with the presence of three crystallographically-inequivalent carbon sites in the fcc unit cell and revealing that the JT-effect dynamics are fast on the NMR time-scale of 10^{-5} s despite the presence of the frozen-in C_{60}^{3-} merohedral disorder disclosed by the ^{133}Cs MAS NMR fine splitting of the tetrahedral and octahedral ^{133}Cs resonances. Cooling to sub-liquid-nitrogen temperatures leads to severe broadening of both the ^{13}C and ^{133}Cs MAS NMR multiplets, which provides the signature of an increased number of inequivalent ^{13}C and ^{133}Cs sites. This is attributed to the freezing out of the C_{60}^{3-} JT dynamics and the development of a t_{1u} electronic orbital glass state guided by the merohedral disorder of the fcc structure. The observation of the dynamic and static JT effect in the Mott insulating state of the metrically cubic but merohedrally disordered Cs_3C_{60} fulleride in different temperature ranges reveals the intimate relation between charge localization, magnetic ground state, lifting of electronic degeneracy, and orientational disorder in these strongly-correlated systems.

Introduction

Alkali fullerides, A_3C_{60} (A = alkali metal) are isotropic high-temperature molecular superconductors with critical temperatures as high as 38 K.[1–6] Because of their molecular nature, these cubic molecular materials are characterized by strong on-site electron correlations and narrow electronic bandwidths, whose relative magnitude is controlled by the intermolecular overlap of t_{1u} orbitals.[1] For the most expanded fullerides, A15- and fcc-structured Cs_3C_{60}, electron correlations prevail and the t_{1u}^3 electrons are localised on the C_{60}^{3-} anions at ambient pressure to produce a Mott insulator. This antiferromagnetic insulator can be driven back to a metallic/superconducting state by compression without any accompanying structural change.[2–4] These recent findings have challenged the standard explanations of fulleride superconductivity within the conventional Bardeen-Cooper-Schrieffer (BCS) framework which relies on electron-phonon coupling for the pairing and brought forward theoretical models in which electron correlations play a prominent role.[7–9]

Approaching the problem from the molecular side, the C_{60}^{3-} ions are potentially unstable towards Jahn-Teller (JT) deformations since the three electrons in the t_{1u} molecular orbitals, whose threefold degeneracy is preserved in the solid state because of the high lattice (cubic) symmetry, can couple to the eight H_g vibrations of the molecular units.[1,10,11] The degeneracy of the t_{1u} orbitals is important in stabilizing the metallic and superconducting state against the Mott insulator in the A_3C_{60} systems by enhancing intermolecular hopping relative to the non-degenerate case and therefore favouring electron delocalisation.[1,12] As the JT-active vibrations are the ones which mediate the electron-phonon coupling,[1,11] they are intrinsically relevant to the study of the competing insulating and metallic/superconducting states in A_3C_{60}.[2–4]

The JT effect (static or dynamic) grows in importance when charges are localized on the C_{60}^{3-} units,[11] thereby making expanded fullerides, such as the two polymorphs of Cs_3C_{60},

model systems to investigate the interplay between the molecular JT effect and Mott electron localization. The relevance of the JT effect in Mott-insulating Cs_3C_{60} was first established indirectly through the observation of a low-spin S = 1/2 ground state despite the retention of cubic symmetry that favoured a high-spin S = 3/2 state for the C_{60}^{3-} anion.[3–5] More recently, subtle changes in the shape of the C_{60}^{3-} ions due to the JT distortion were directly observed by infrared (IR) spectroscopy.[11] These experiments revealed that the transition to the localized state in both A15- and fcc-structured Cs_3C_{60} polymorphs is accompanied by a loss of the triple degeneracy of the t_{1u} frontier orbital via the dynamic JT effect at temperatures up to 400 K. The upper limit for the rate of inter-conversion between different JT-distorted conformers is on the order of 10^{11} s^{-1}, that is the distortion is observed as static on the time-scale of the IR measurements. Strong coupling to the vibrational H_g modes of C_{60} leads to the warping of the adiabatic potential energy surface, which is very small according to recent calculations on single orientations of C_{60}^{3-} anions and thus the dynamic JT effect is theoretically predicted to be stable at all temperatures.[13]

However, the presence of local symmetry breaking terms may deepen some minima of the adiabatic potential energy surface[10] leading to an effectively static JT distortion depending on the timescale of the measurement and the observation temperature. In insulating non-cubic fullerides, in which the crystal field is strong enough to select the particular fulleride distortion, the role of the JT effect in tuning the nearest neighbour C_{60}-C_{60} exchange interactions has been well established.[14] For instance, the presence of the static JT effect is necessary to explain the appearance of ferromagnetism in TDAE-C_{60} (TDAE ≡ tetrakis(dimethylamino)ethylene),[15,16] of antiferromagnetism in Mott-insulating $(NH_3)K_3C_{60}$ [17,18] and $(CH_3NH_2)K_3C_{60}$,[14,19–22] and of spin-singlet states in A_4C_{60} phases.[23,24]

Therefore, discussion of the JT effect in cubic Mott-insulating and metallic/superconducting A_3C_{60} phases should also take into consideration the possible freezing of the dynamics of the molecular JT deformations driven by the local site disorder. Such intrinsic disorder is present in fcc A_3C_{60} (space group $Fm\bar{3}m$), which is merohedrally disordered (Fig. 1a) – there are two equally populated standard C_{60} orientations related by a 90° rotation about the [001] or equivalently by 44°23' about the [111] crystal axes.[25] In order to unveil the metal coordination with the C_{60}^{3-} ions, local probe techniques, such as alkali-metal or ^{13}C NMR, have been employed. In particular, two alkali ions per C_{60} occupy the tetrahedral (T) and one the octahedral (O) sites.[25] This leads to an expected intensity ratio of 2:1 for the two peaks, T and O in static alkali-metal NMR spectra, as indeed observed for metallic/superconducting Rb_3C_{60} at high temperatures (>440 K).[26] However, on cooling, the peak associated with the tetrahedrally coordinated ions splits into two components (labeled as T and T') although the crystal structure is still consistent with the presence of a single tetrahedral alkali ion. Due to the correlation between the temperature at which the C_{60}^{3-} units start to rotate on the NMR time-scale and the temperature above which the T-T' doublet collapses into a single peak, the splitting has been associated with the merohedral disorder.[26–30]

Magic angle spinning (MAS) NMR probes the local environment of nuclei with the highest resolution and is thus ideally suited for the investigation of the origin of the T-T' doublet structure in the static NMR spectra of fcc A_3C_{60}, which violates the crystal symmetry expectations. Indeed, ^{87}Rb MAS NMR experiments at room temperature on metallic Rb_3C_{60} reveal an even more complex picture where – in addition to the T' resonance – the main T peak is further split into two overlapping lines,[30,31,32] which can also be accounted for by the local variation of the Rb^+ tetrahedral environment as the surrounding C_{60}^{3-} ions take one of the two available standard C_{60} orientations but without localization of JT distortions.[30] However, if merohedral disorder effects are of importance, they should be also accompanied by multiplet splitting of the O-site resonance. The appearance of a secondary O' resonance was noted in the ^{87}Rb MAS NMR spectra of Rb_3C_{60} [30,31] without any further discussion.

The freezing of the dynamics of the molecular C_{60}^{3-} deformations in merohedrally disordered insulating fcc Cs_3C_{60} would additionally reduce the local site symmetries thus leading to additional splittings of the ^{13}C and ^{133}Cs NMR peaks. However, such subtle changes are difficult to follow by conventional static ^{13}C or ^{133}Cs NMR spectroscopy at low temperatures due to the large anisotropic broadening,[3–5] necessitating again the use of MAS NMR.

Advances in probe design have recently made possible extension of MAS NMR experiments down to cryogenic temperatures.[33–37] Here we make use of these newly presented opportunities to investigate the fcc-structured Mott-insulating Cs_3C_{60} by ^{13}C and ^{133}Cs MAS NMR spectroscopy to sub-liquid-nitrogen temperatures allowing us to address two important open issues: (i) how the JT effect interacts with the intrinsic orientational disorder imposed by the presence of the two standard orientations of the C_{60}^{3-} anion and (ii) whether static JT distortions can occur at low temperatures without a cooperative JT transition to a long-range ordered state. These points are fundamental in understanding the link between the electronic structure of the C_{60}^{3-} anion, the average crystal structure probed by diffraction techniques and the resulting cooperative electronic and magnetic properties of the extended molecular solid, as the orbital degeneracy of C_{60} is intimately related to the energies of the competing metallic and insulating states. The high-resolution of our experiments reveals the variations in local Cs^+ coordination associated with the C_{60}^{3-} merohedral disorder and the dynamic JT effect. On cooling we find that the number of inequivalent ^{133}Cs and ^{13}C sites increases drastically in a correlated fashion despite the retention of long-range crystallographic fcc symmetry. This is consistent with the freezing out of the C_{60}^{3-} JT deformations on the NMR time-scale of 10^{-5} s and the formation of merohedral-disorder-induced randomly-oriented frozen t_{1u} orbital arrangements at low temperature. Thus, the low temperature electronic structure of the magnetic Mott-insulating state, which on pressurization produces the highest T_c seen in a molecular system, emerges as

that of a JT orbital glass, reflecting the interplay between lattice disorder, orbital degeneracy and ground spin state of the C_{60}^{3-} anion.

Experimental Methods

Sample preparation and characterization

The fcc Cs_3C_{60} powder sample used in the present work was prepared according to the procedure reported elsewhere (sample 1 of Ref. [4]). Synchrotron X-ray powder diffraction (XRPD) showed that the phase fraction of fcc Cs_3C_{60} is 86%. The fractions of minority co-existing A15-structured Cs_3C_{60}, body-centered orthorhombic (bco) Cs_4C_{60}, and CsC_{60} phases are 3%, 7%, and 4%, respectively.[4]

NMR spectroscopy

^{133}Cs (nuclear spin I = 7/2) and ^{13}C (I = 1/2) MAS NMR experiments were performed at a magnetic field of 8.5 T. Complementary static ^{133}Cs and ^{13}C NMR spectra were measured in a magnetic field of 9.4 T. The ^{133}Cs and ^{13}C NMR signals were referenced to those of 0.1 M solutions of $CsNO_3$ and hexamethyldisiloxane in D_2O with Larmor frequencies of 47.1752 MHz and 90.4393 MHz, respectively. The ^{13}C NMR shifts were recalculated with respect to the tetramethylsilane (TMS) standard to allow direct comparison with literature data. ^{133}Cs MAS NMR spectra were measured at the spinning frequency of ν_R = 25 kHz. The Hahn-echo pulse sequence with an optimized ^{133}Cs 90° pulse length of 8 µs, an interpulse delay of 32 µs, and a repetition time of 0.4 s was employed in the temperature dependent experiments. ^{13}C MAS NMR spectra were also measured at spinning frequencies ν_R = 25 kHz with a Hahn-echo pulse sequence (90° pulse length of 5 µs, interpulse delay of 45 µs, and repetition time of 0.2 s). Cryogenic MAS (cryoMAS) NMR experiments in the temperature range 300 to 51 K employed a home-built 1.8 mm cryoMAS probe with appropriate temperature calibration.[33–37]

Spin-lattice relaxation times, T_1, were measured only at room temperature for both nuclei by applying a saturation-recovery Hahn-echo pulse sequence. In the ^{13}C experiments, a saturation train consisted of 20 pulses each of 7 µs in length and a 200 µs delay inbetween, while in the ^{133}Cs experiments, the saturation train consisted of 80 pulses each of 10 µs in length and a 150 µs delay inbetween. The longest delay between saturation pulse train and Hahn-echo was at least three times longer than the extracted T_1. The recovery of nuclear magnetization was successfully simulated for individual resonances by single exponential terms.

Results

Dynamic Jahn-Teller effect at high temperature

In Cs_3C_{60}, the merohedral disorder is completely frozen-in on the NMR time-scale at 380 K – the highest temperature of our experiments (Fig. S1)[38] – as the large Cs^+ ions occupying the small tetrahedral interstices completely block the C_{60}^{3-} reorientational motion. The freezing temperature is higher than those in less expanded A_3C_{60} systems. For instance, in Rb_3C_{60} and K_3C_{60} the large amplitude rotations of the C_{60}^{3-} anions between the two standard orientations slow down on the NMR time-scale in the temperature intervals of 380-300 K and 230-200 K, respectively.[29,31] At room temperature, the static ^{13}C NMR spectrum of fcc Cs_3C_{60} (Fig. 1) shows a full powder anisotropy with components $\delta_{\parallel}$ = 335(5) ppm and $\delta_{\perp}$ = 125(5) ppm and an isotropic shift of δ_{iso} = 196(5) ppm for the uniaxial shift tensor. The observation of such a powder lineshape unambiguously confirms that the C_{60}^{3-} ions are indeed static on the NMR time-scale.

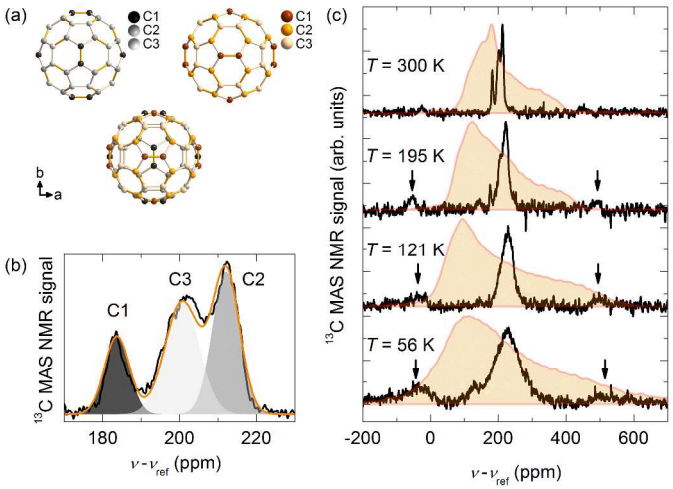

Figure 1: (a) Two equally populated standard C_{60} orientations (top) related by a 90° rotation about the [001] or equivalently by 44°23' about the [111] crystal axes in the $Fm\bar{3}m$ average structure of Cs_3C_{60} (bottom). Carbon atoms at (0, 0.0491, 0.2407), (0.2051, 0.0767, 0.0987) and (0.1764, 0.1533, 0.0503) crystallographic positions contributing to C1, C2 and C3 ^{13}C MAS NMR peaks are marked for both standard orientations, respectively. (b) ^{13}C MAS NMR spectrum measured at room temperature (solid black line) and its fit to three Gaussian components in the intensity ratio, C1:C2:C3 = 1:2:2 (orange line; the grey shaded areas depict the C1, C2, and C3 spectral components). (c) Temperature dependence of the ^{13}C MAS NMR spectra of fcc Cs_3C_{60}. The corresponding static ^{13}C NMR spectra (shaded areas – data taken from Ref. 4) are shown for comparison. Spinning sidebands (marked with arrows) on both sides of the center band resonance are visible below ~200 K.

Rapid spinning of the sample at ν_R = 25 kHz in the ^{13}C MAS NMR experiment effectively averages out all the anisotropic interactions between the ^{13}C nuclei and the electrons on the C_{60}^{3-} ion revealing a spectrum (Fig. 1b) that consists of three clearly resolvable peaks with centers at 212.1(5) ppm (peak labeled as C2), 200.7(5) ppm (C3) and 183.7(5) ppm (C1). The average shift [200(1) ppm] fall into the expected range for C_{60}^{3-} ions and is in agreement with the isotropic shift of the corresponding static ^{13}C NMR spectrum.[4] An excellent description of the measured spectrum is achieved by fitting it to a three-Gaussian component (C1, C2, and C3) function in

which the ratio of the relative intensities is fixed to 1:2:2, respectively (Fig. 1b). The multiplicities of the three chemically inequivalent carbon sites in the $Fm\overline{3}m$ structure are 96, 192, and 192, respectively, matching the 1:2:2 relative intensity ratio of the observed C1, C2, and C3 ^{13}C NMR peaks. Taking into account the relative peak intensities and consideration of the C_{60}^{3-} t_{1u} charge densities at the carbon sites[39,40] allows assignment of the three peaks to carbons at the (0, 0.0491, 0.2407), (0.2051, 0.0767, 0.0987) and (0.1764, 0.1533, 0.0503) crystallographic positions (Fig. 1a), respectively.[4]

Such a triplet structure has never been observed before by ^{13}C MAS NMR in any of the metallic A_3C_{60} fullerides. Instead a single resonance is invariably observed[41] despite the existence of three chemically inequivalent carbon sites in the crystallographic $Fm\overline{3}m$ space group.[25] The experiments on the expanded Mott-insulating Cs_3C_{60} in which the large Cs^+ ions in the tetrahedral sites freeze the C_{60}^{3-} rotations and at the same time enhance the cubic crystal field allow us for the first time to probe the C_{60}^{3-} electronic structure and dynamics at high resolution. The observation of three ^{13}C MAS NMR resonances is consistent with the $m\overline{3}$ (T_h) molecular symmetry of each of the two standard orientations of the C_{60}^{3-} ions in Cs_3C_{60} – this directly demonstrates that the symmetry of the t_{1u} molecular orbitals is not broken locally and that no molecular deformations are detectable at room temperature. The absence of local symmetry reduction therefore implies that, although the reorientational motion of the merohedrally-disordered fulleride ions is frozen on the NMR time-scale of 10^{-5} s with each unit randomly adopting one of the two standard orientations (orientational glass state), the interconversion between possible JT-deformed fulleride ions is fast enough to time average the molecular distortion of individual C_{60}^{3-} units and restore the molecular site symmetry and t_{1u} electronic orbital degeneracy (orbital liquid state). The molecular JT effect in fcc Cs_3C_{60} is thus dynamic in nature at room temperature with a time-scale of interconversion between solid-state conformers shorter than the NMR time-scale of 10^{-5} s but longer than the IR time-scale of 10^{-11} s.

Crossover from dynamic to static Jahn-Teller deformed molecular units on cooling

Transition from the dynamic to the static JT deformation regime is expected to multiply the number of inequivalent ^{13}C sites because the charge density varies considerably over the distorted C_{60} units.[15,16] For instance, the JT-driven deformation of C_{60}^{3-} with the highest possible orthorhombic site symmetry (*mmm*) has D_{2h} symmetry[11,42] would show 9 individual ^{13}C NMR lines, *i.e.* the C1-C3 peaks would split further into three components each. The three ^{13}C MAS NMR peaks present at room temperature can be still resolved down to 195 K – despite a gradual increase in linewidth of the individual components on cooling – so both the $m\overline{3}$ site symmetry and the t_{1u} orbital degeneracy of C_{60}^{3-} are retained in this temperature interval. On further cooling, the continuously increasing peak broadening leads to considerable overlap and the ^{13}C NMR spectra at 167 and 144 K collapse into a single line whose triplet structure is only evident by the presence of shoulders. The asymmetry of the ^{13}C MAS NMR line is no longer discernible at 121 K and below (Fig. 1c). The observed peak broadening cannot be ascribed to reasons of technical origin as spinning of the sample at ν_R = 25 kHz proceeded smoothly at all temperatures and consequently, the anisotropic electron-nuclear dipolar interaction responsible for the broadening of the static ^{13}C NMR spectra is effectively averaged out. We note that the partial shift of the resonance signal intensity below 195 K into the spinning sidebands, which flank the center band resonance, should also have no effect on the width of the ^{13}C MAS NMR resonances.[43] Therefore, the pronounced ^{13}C MAS NMR peak broadening between 195 and 121 K can only be interpreted as additional splitting of the C1-C3 peaks linked to a physical process associated with the C_{60}^{3-} anions that are slowing down before eventually freezing out on the NMR time-scale in this temperature interval. This process is responsible for the observation of a single very broad central band that implies a wide distribution of ^{13}C NMR shifts and directly demonstrates that the molecular symmetry is lower than $m\overline{3}$ below 121 K.

The low temperature ^{13}C MAS NMR spectra clearly reveal the presence of more than three chemically inequivalent carbon sites. This contrasts with the results of high-resolution synchrotron X-ray diffraction experiments, which show retention of $m\overline{3}$ symmetry at all temperatures down to 5 K.[4] We conclude that the observed molecular symmetry-breaking must be local and random in nature to preserve the global crystallographic symmetry on the X-ray scattering length scale. As the C_{60} molecular rotations are frozen on the NMR time-scale, changes in the merohedral disorder as the origin of the observed spectral changes can be ruled out. In addition, although fcc Cs_3C_{60} is very close to the insulator-to-metal boundary[4,44–47] where charge fluctuations could lead to strong variations in the local electronic environment,[48] the sample remains insulating at all temperatures, thus eliminating this possibility too.

The remaining candidate as the source of the NMR spectral broadening is the JT distortion of the C_{60}^{3-} molecular ions. Static (on the NMR time-scale of 10^{-5} s) JT deformations of the C_{60}^{3-} units will considerably multiply the number of inequivalent ^{13}C resonances. In the most symmetric D_{2h} JT-driven deformation of the fulleride ions, the C_2 rotation axes act as principal axes of distortion.[42] As the fulleride ions contain 15 such twofold axes, 30 distortions are possible with the same shape but with the principal axis oriented in different directions.[11] The resulting distribution of the ^{13}C NMR shifts is then manifested as a severe broadening of the three-individually resolved ^{13}C peaks, which all overlap into a single broad resonance at low temperature (Fig. 1c). Therefore, the ^{13}C MAS NMR response below 195 K where individual ^{13}C peaks gradually broaden with decreasing temperature allows us to track the crossover from dynamic JT distortion to static JT freezing in the multitude of possible JT deformations of the C_{60}^{3-} units. Very importantly, the symmetry breaking will lift the degeneracy of the t_{1u} orbitals, which span three separate

representations (b_{1u}+b_{2u}+b_{3u}) in D_{2h} symmetry. This finding has not been anticipated before, as theoretical investigations of expanded A_3C_{60} systems in the absence of orientational disorder predict that the dynamic JT effect survives at all temperatures.[8,13] Therefore, we propose that the presence of a frozen merohedrally disordered C_{60}^{3-} lattice locally stabilizes differently directed JT distortions leading to local minima in the adiabatic potential energy surface. In order to unveil the role of the merohedral disorder in defining the electronic state of fcc Cs_3C_{60} we next turn to ^{133}Cs MAS NMR measurements.

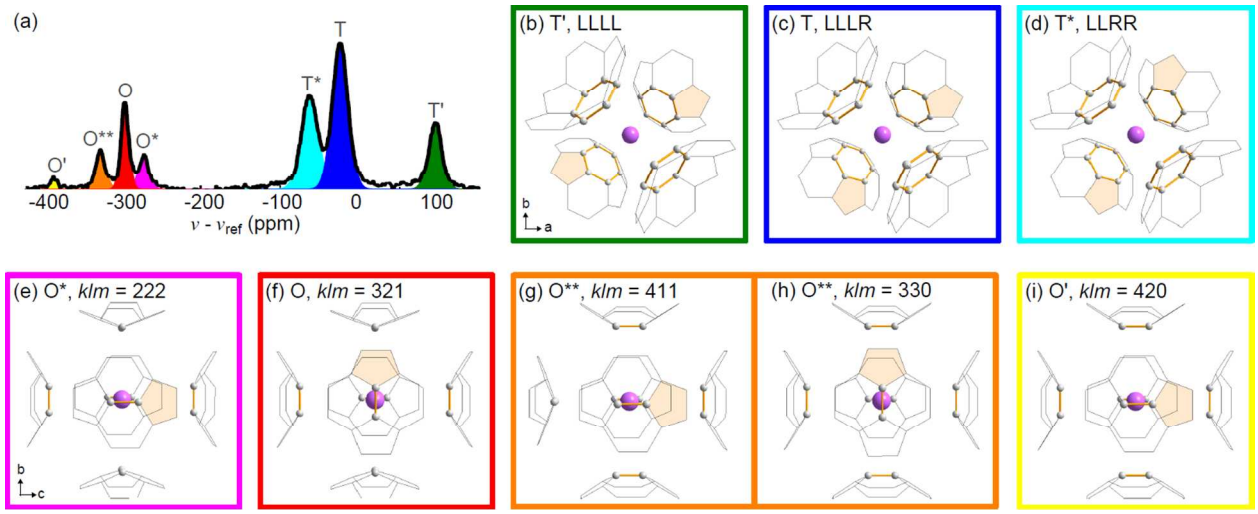

Figure 2: Splitting of ^{133}Cs MAS NMR spectra (ν_R = 25 kHz) of fcc Cs_3C_{60} due to the merohedral disorder. The assignment of the high-resolution ^{133}Cs MAS NMR peaks measured at room temperature (a) to different tetrahedral (b-d) and octahedral site (e-i) coordinations. In (b), the tetrahedral Cs^+ ion lies directly above the centers of four hexagonal faces of neighboring C_{60}^{3-} ions which adopt the same standard orientation (configuration LLLL). In (c), one of the C_{60}^{3-} ions is in the second standard orientation (configuration LLLR). The additional distinct configuration (LLRR, two C_{60}^{3-} ions in each of the two standard orientations) for the tetrahedral Cs^+- C_{60}^{3-} contacts is depicted in (d). In (e), the octahedral Cs^+ ion lies directly above the midpoints of six 6:6 bonds of neighboring C_{60}^{3-} ions which adopt the same standard orientation (configuration 222). In (f), one of the C_{60}^{3-} ions is in the second standard orientation (configuration 321). The three additional distinct configurations (330, 411, and 420) for the octahedral Cs^+-C_{60}^{3-} contacts are depicted in (g-i).

The coordination environments of the alkali metal ions

The ^{133}Cs MAS NMR spectrum of fcc Cs_3C_{60} at room temperature is shown in Fig. 2a. It consists of 7 lines, whose positions coincide with those of the three broad O, T and T' resonances previously observed in the static NMR measurements.[4,44,45] The splitting directly reflect local violations of the crystallographic 23 and $m\bar{3}$ symmetry of the T and O sites, respectively. The high resolution of the MAS NMR experiments allows us to resolve a further component, T* at –63.2(1) ppm in addition to the T and T' peaks at –24.6(1) and 94.8(1) ppm, respectively. The spectral region corresponding to the octahedral site shows an even more complex substructure. In addition to the main O [–295.3(1) ppm] and O' (–384.8(2) ppm) peaks observed in static NMR spectra, two additional weaker lines, O* and O** are present at –272.1(1) and –326.2(1) ppm, respectively. The three-component structure of the alkali T resonance observed before[31,30,32] in the ^{87}Rb MAS NMR spectra of metallic Rb_3C_{60} is thus also resolved in isostructural Mott-insulating Cs_3C_{60}. However, ^{133}Cs MAS NMR in Cs_3C_{60} also shows pronounced fine structure for the alkali O resonance, a feature which was absent in previous NMR experiments on metallic A_3C_{60}.

To understand such a complex ^{133}Cs MAS NMR spectrum, we consider the merohedrally disordered $Fm\bar{3}m$ Cs_3C_{60} structure when the reorientational dynamics of the C_{60}^{3-} anions are already frozen, but the JT molecular deformation interconversions are still fast on the NMR time-scale. The coordination environment of the alkali metal ions in the tetrahedral and octahedral interstices in a hypothetical orientationally ordered A_3C_{60} fcc structure is shown in Figs. 2b and 2e, respectively. In the tetrahedral site, each alkali ion lies directly above the centers of hexagonal faces of neighboring C_{60}^{3-} whose unique orientation is denoted L. However, in the merohedrally disordered A_3C_{60} fcc structure,[25] a second equally populated C_{60} standard orientation (denoted R) modifies the alkali metal coordination environment. If we label the T-site ion coordination environment as LLLL when all four C_{60} neighbors adopt the same standard orientation (Fig. 2b), there will be two further distinct environments possible: those with three L and one R orientation (LLLR, Fig. 2c) and with two L and two R orientations (LLRR, Fig. 2d). Similarly, the A^+ ions in the octahedral site lie directly above the midpoints of C_{60} C–C bonds fusing two hexagons (6:6). Because of the merohedral disorder, there are two equally-probable nearest A^+-C_{60}^{3-} contacts to two 6:6 fusions of each of the six nearest

neighboring fulleride ions related by a 90° rotation.[25] We thus use the orientations of these 6:6 fusions of C_{60} units to label the local O-site coordination by introducing a three-digit configuration number *klm* (*k*+*l*+*m* = 6), which specifies the number of 6:6 fusions around each O site directed along the *x*-, *y*-, and *z*-direction, respectively. For the hypothetical fully orientationally ordered A_3C_{60} fcc structure, the O-site configuration label is *klm* = 222 as there are two 6:6 bonds aligned along each of the three crystallographic axes (Fig. 2e). However, when one of the six C_{60}^{3-} neighboring ions is in the second standard orientation, its contact 6:6 bond will be rotated by 90° about one of the crystal axes (Fig. 2f) and the corresponding configuration label will be 321. In this way one can also construct the remaining three octahedral coordinations, 330, 411, and 420 depicted in Figs. 2g-i. Each of these local tetrahedral and octahedral A^+ coordinations contributes to a distinct NMR peak (Fig. 2a) whose relative intensity depends on the configuration probability. Comparison of the ^{133}Cs O and T peak intensities (Table S1)[38] with the probabilities for different L and R combinations[30] and *klm* configuration numbers (Table S2)[38] shows a good agreement and allows us to assign each individual peak to a different alkali metal merohedrally disordered C_{60}^{3-} environment (Fig. 2a). Therefore, the merohedral disorder model can consistently account for the complex structure of the room temperature high-resolution ^{133}Cs MAS NMR spectrum of fcc Cs_3C_{60}. The clear relation established between the multiple O and T-site derived lines and the local fields generated by proximity of the Cs^+ ions to the different C atoms in the different merohedral-disorder-derived local arrangements makes the evolution of the ^{133}Cs spectrum with temperature a sensitive probe of changes in local structure at the C_{60}^{3-} site. Therefore, we next evaluated the temperature dependence of the ^{133}Cs MAS NMR.

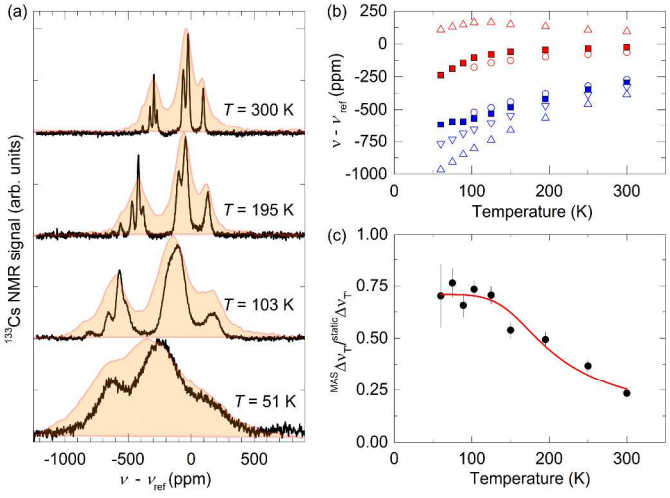

Figure 3: (a) Temperature dependence of the ^{133}Cs MAS NMR spectra (ν_R = 25 kHz) of fcc Cs_3C_{60}. The corresponding static ^{133}Cs NMR spectra (shaded areas – data taken from Ref. 4) are included for comparison. (b) Temperature dependence of the ^{133}Cs MAS NMR shifts of the components of the tetrahedral (T, red) and octahedral (O, blue) peak manifolds [T' (triangles), T (squares), T* (circles), O* (circles), O (squares), O** (inverted triangles), O' (triangles)]. (c) Temperature dependence of the ratio between the width of the isolated ^{133}Cs MAS NMR T' line, $^{MAS}\Delta\nu_{T'}$, and the corresponding static ^{133}Cs NMR T' linewidth, $^{static}\Delta\nu_{T'}$. The red solid line is a fit to thermally activated Jahn-Teller dynamics (see text for details) yielding an activation energy of E_{JT} = 68(15) meV.

Coupling between merohedral disorder and JT dynamics

The broadening of the ^{13}C MAS NMR peaks with decreasing temperature provides the signature of the gradual slowing down and eventual freezing out of the JT dynamics as established above. However, it remains to be investigated if and how the individual JT deformations adapt to the underlying background of static merohedral disorder. The temperature dependence of the ^{133}Cs MAS NMR spectra of fcc Cs_3C_{60} between 300 and 51 K is compared with that of the static NMR spectra in Fig. 3a. The general multiplet structure of ^{133}Cs MAS NMR spectra persists at all temperatures, but individual peaks shift strongly (Fig. 3b) and broaden considerably so they can be followed only by spectral fitting (Figs. S2)[38] as the temperature decreases. The persistence of the fine structure of the O and T ^{133}Cs resonances clearly reflects the robustness of the C_{60}^{3-} merohedral disorder – the C_{60}^{3-} anions remain randomly and equally distributed between the two standard orientations as the temperature is lowered. The observed peak broadening on cooling cannot be ascribed to reasons of technical origin as spinning of the sample proceeded smoothly at all temperatures and consequently, the anisotropic electron-nuclear dipolar interaction is effectively averaged out. On the other hand, the local site disorder can lift the high symmetry of the T and O ^{133}Cs sites and in principle quadrupole interaction, which could make a contribution to the observed ^{133}Cs MAS NMR broadening, is present. However, no satellite transitions are observed in the static ^{133}Cs NMR spectra[4] setting an upper limit of $\nu_Q \leq 2$ kHz for the quadrupole frequency of such distorted sites and confirming that the first order quadrupolar broadening of the ^{133}Cs MAS spectra is also effectively removed by the magic angle spinning.

Individual T and O peak components can be followed down to 103 K. However, due to the pronounced peak broadening, the T* and O* peaks can no longer be resolved below 103 K. At 51 K, the broadening is so severe that only the main O, T, and T' peaks can be recognized and the ^{133}Cs MAS NMR spectrum resembles the static ^{133}Cs NMR spectrum (Fig. 3a).[4] The broadening of the ^{133}Cs MAS NMR peaks (Fig. S3)[38] is so large that the widths of the main O and T peaks approach those deduced from the static ^{133}Cs NMR experiments. For instance, for the most isolated T' peak, the width of the ^{133}Cs MAS NMR line, $^{MAS}\Delta\nu_{T'}$, at room temperature is 0.23(2) of the corresponding static ^{133}Cs NMR linewidth, $^{static}\Delta\nu_{T'}$ (Fig. 3c). The ratio, $^{MAS}\Delta\nu_{T'}/\ ^{static}\Delta\nu_{T}$ between the two linewidths smoothly increases on cooling and approaches ~0.7 below 125

K. This shows that the pronounced peak broadening of the ^{133}Cs MAS NMR resonances on cooling directly mirrors an increasing spread of the ^{133}Cs shifts. Very importantly, the comparable temperature dependence of the ^{13}C and ^{133}Cs MAS NMR broadening (Fig. S3)[38] suggests that they are correlated and both have the same physical origin. Since the former probes the charge distribution on the C_{60}^{3-} units, while the latter is more sensitive to the C_{60}^{3-} orientational disorder, we conclude that the merohedral disorder and the JT dynamics are strongly coupled with the former providing a frozen background against which the JT conformational dynamics evolve on cooling.

Discussion

The importance of the robust merohedral disorder, present in the fcc Cs_3C_{60} crystal structure, in determining its electronic properties is immediately apparent if we consider the simplest orientationally ordered version, namely when bidirectional order of the two standard C_{60}^{3-} orientations (Fig. 1a) occurs. The resulting structure is tetragonal (space group $P4_2/mnm$)[49] with a unique axis that will locally drive the JT deformations of C_{60}^{3-} anions to select a well-defined direction. Such a unique axis is absent in the orientationally disordered cubic structure which is consistent with the JT effect being dynamic at all temperatures without structural distortions associated with cooperative static orbital order. The frozen merohedral disorder of the C_{60}^{3-} ions locally breaks the crystal symmetry on sub-XRD length scales, thus randomly creating minima in the adiabatic potential energy surfaces that make the JT deformations inequivalent and affect their dynamic interconversion. Since the merohedral disorder freezes out first well above room temperature (Fig. S1)[38], it also forces the JT deformations to be random when they themselves freeze out on the NMR time-scale. The disordered merohedral "background", demonstrated by the ^{133}Cs MAS measurements, within which the freezing of the JT dynamics takes place, prevents the identification of a "consensus" direction for the local deformation axes to align with. Because any correlations between the merohedrally disordered orientations are on sub-XRD length scales as shown by the retention of cubic $Fm\bar{3}m$ symmetry, this eliminates any possibility of a cooperative JT effect and prevents a global crystallographic symmetry change. The low-temperature electronic state of Mott-insulating Cs_3C_{60} should be thus regarded as that of a JT orbital glass.

Additional quantitative information on the JT dynamics can be derived from the temperature dependence of the ^{133}Cs MAS NMR lineshifts and linewidths (Fig. 3b,c). The Curie-Weiss-like temperature dependence of the shifts of all O peaks (Figs. 3b and S4)[38] is consistent with the insulating behavior of fcc Cs_3C_{60}.[4,44,45] However, the temperature response of the T- and T'-peak lineshifts is distinctly different. While at high temperature Curie-Weiss behavior is obeyed, we observe a sudden deviation from this trend below 125 K. We recall that complementary bulk experimental techniques, such as diffraction and magnetometry, do not detect any anomaly in this temperature range.[4] Since the shift of ^{133}Cs NMR peak is given by the isotropic hyperfine coupling to the neighboring C_{60}^{3-} moments, the anomalous behavior should be associated with local JT-effect-induced electronic or structural changes that are probed only by high-resolution MAS NMR of the tightly packed ^{133}Cs in the tetrahedral interstices. The linewidths of the T and T' peaks also show a pronounced temperature response (Fig. S3)[38] increasing monotonically with decreasing temperature with the ratio, $^{MAS}\Delta\nu_{T'}/\ ^{static}\Delta\nu_{T'}$ saturating at ~0.7 below 125 K (Fig. 3c). This clearly reveals the additional low-temperature splitting of the Cs peaks beyond what is consistent with the merohedral disorder and the $m\bar{3}$ symmetry of C_{60}^{3-} (*vide infra*) and fully supports the conclusions on the freezing-out of the dynamics of JT deformations of C_{60}^{3-} anions derived from the ^{13}C MAS NMR (Fig. 1). The crossover from the high-temperature regime where $^{MAS}\Delta\nu_{T'}/\ ^{static}\Delta\nu_{T'} << 1$ to that where $^{MAS}\Delta\nu_{T'}/\ ^{static}\Delta\nu_{T'}$ saturates at values close to 0.7 also explains why the ^{133}Cs MAS and static spectra nearly coincide at 51 K (Fig. 3a).

The linewidth of the static ^{133}Cs NMR spectrum has two main contributions: the anisotropic dipolar interactions between the C_{60}^{3-} electrons and the ^{133}Cs nuclei and the contribution arising from the JT-induced distribution of the isotropic hyperfine coupling constants. Both contributions are proportional to the static spin susceptibility, χ, and the linewidth of the T' peak can be written as the sum of the individual second-moment contributions: $^{static}\Delta\nu_{T'} = (a_{dip}^2 + \langle a_{iso}^2 \rangle)^{1/2}\chi$, where a_{dip} is the electron-nuclear dipolar part of the anisotropic hyperfine coupling and $\langle a_{iso}^2 \rangle$ is the mean square distribution of the ^{133}Cs isotropic coupling constants, a_{iso}. In the MAS NMR experiments, the anisotropic dipolar interactions are effectively averaged out by the rapid magic angle spinning, and therefore: $^{MAS}\Delta\nu_{T'} = \langle a_{iso}^2 \rangle^{1/2}\chi$. The ratio of the two linewidths plotted in Fig. 3c is thus

$$^{MAS}\Delta\nu_{T'}/^{static}\Delta\nu_{T'} = [\langle a_{iso}^2 \rangle / (a_{dip}^2 + \langle a_{iso}^2 \rangle)]^{1/2}. \qquad (1)$$

The temperature dependence of $\langle a_{iso}^2 \rangle$ arises from the evolution of the thermally activated JT dynamics and is given by the expression[50] $\langle a_{iso}^2 \rangle = \langle a_{iso}^2 \rangle_0 \tan^{-1}[\delta\omega\ \tau_c]$. Here $\langle a_{iso}^2 \rangle_0$ is the magnitude of the distribution of isotropic hyperfine coupling constants imposed by the static JT deformations. $\delta\omega/2\pi \approx 12.8$ kHz is the homogeneous linewidth corresponding to a T' linewidth of 270 ppm at low temperature (Fig. S3)[38], and $\tau_c = \tau_0 \exp(E_{JT}/k_BT)$ is the temperature-dependent correlation time for the JT dynamics. Fitting the temperature dependence of $^{MAS}\Delta\nu_{T'}/\ ^{static}\Delta\nu_{T'}$ (Fig. 3c) to the above expressions yields an energy barrier, E_{JT} = 68(15) meV and a pre-exponential factor, $\tau_0 \approx 1\times10^{-7}$ s. The extracted value of the energy barrier is distinctly different from that of the C_{60}^{3-} anion reorienational motion [~580 meV for Rb_3C_{60} [29]] and falls into the energy range expected for the JT effect.[8] Thus E_{JT} represents the energy barrier for the uncorrelated thermally activated jumps between different JT conformer states with correlation times that match the experimental NMR time-window between ~200

and 100 K. We note that the above model is the simplest possible interpretation of the data in order to estimate E_{JT}: it does not consider tunneling effects or any possible temperature dependence in E_{JT} due to changes in the local crystal field because of lattice expansion.

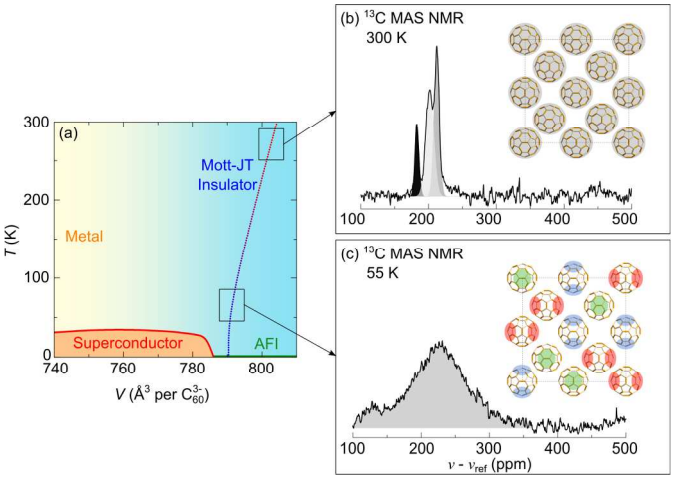

Figure 4: (a) Electronic phase diagram of fcc A_3C_{60} fullerides shown as a function of volume occupied per C_{60}^{3-} ion. The red solid line shows the superconducting transition temperature, T_c and the green solid line the antiferromagnetic ordering temperature, T_N.[4] The dotted line delineates the temperature evolution of the volume occupied per C_{60}^{3-} ion in fcc Cs_3C_{60} at ambient pressure[4] and marks the path along which the present temperature-dependent MAS NMR measurements were undertaken. The line is color-coded to indicate how the correlation time for the Jahn-Teller deformational dynamics compare with the time-scale of the MAS NMR experiments (10^{-5} s) – at high-temperatures, this timescale is significantly shorter (red color) but as the temperature is lowered it becomes longer (blue color). Open rectangles mark two representative regions of the phase diagram, where the MAS NMR results reveal different dynamics of the Jahn-Teller effect as depicted in (b) and (c). (b) At high temperatures in the Mott-Jahn-Teller-insulating phase,[53] the rate of interconversion between different Jahn-Teller conformers is very fast on the NMR time-scale (orbital-liquid state) thus restoring the high symmetry of the C_{60}^{3-} site and allowing for the observation of three distinct ^{13}C MAS NMR peaks assigned to the C1, C2 and C3 crystalographically inequivalent carbon sites. (c) As the rate of the Jahn-Teller dynamics slows down at low temperatures, the $m\bar{3}$ molecular symmetry is locally broken leading to the multiplication of the number of inequivalent carbon sites with different local molecular distortions and different charge densities, which are marked schematically by the red, blue and green regions of the C_{60}^{3-} units. As a result, a very broad featureless ^{13}C MAS NMR spectrum is measured at 56 K. In this regime, the merohedral disorder removes the degeneracy in the energy of the Jahn-Teller distortions and freezes-in the randomness of the JT conformations leading to a Jahn-Teller orbital glass state.

The static ^{133}Cs NMR second moment is almost temperature independent below 50 K (ignoring the contribution from the development of short-range spin ordering below 15 K).[4] This coincides with the results of the IR experiments,[11] which derived the upper limit of the difference in energy of competing JT conformers as 2.4 meV (28 K). The present MAS NMR results thus establish fully the energy landscape for the C_{60}^{3-} JT deformations in fcc Cs_3C_{60}: the larger energy scale of 68(15) meV is the energy barrier required for the thermally excited jumps between different JT conformers whose energies differ by only 2.4 meV. Although the onset of the static JT effect will lead to the loss of the stabilization energy associated with delocalization of the distortion orientation, the static component will remain[13] providing an energy gain associated with the splitting of t_{1u} levels in the local orientationally-disordered environment.

The presence of the JT effect is common to many strongly correlated solids. For instance, in the high-T_c cuprates the suppression of the cooperative JT effect on chemical doping, and its contribution to the local polaronic effects when structural disorder is introduced into the lattice by this doping, is both important and incompletely understood.[51,52] Expanded fcc Cs_3C_{60} offers a unique chance to investigate how structural disorder couples to JT active electronic degrees of freedom in the vicinity of the insulator-to-metal boundary because the molecular nature of the parent states protects their degeneracy in the cubic lattice. The Cs_3C_{60} insulator has Mott-like properties, with an interesting interplay between electron-electron repulsion and the JT effect leading to the Mott-Jahn-Teller-insulating state (Fig. 4a).[53] Due to the large thermal expansion of this molecular solid, we start the experiment at room temperature deep in the insulating state, but end up extremely close to the metallic and superconducting phase boundary at low temperatures. The merohedral disorder, frozen-in already well above room temperature, locally perturbs the cubic crystal field thus opening an energy difference between the different static conformers of about 2.4 meV. The C_{60}^{3-} ions rapidly transform between different conformers by thermally exciting over the much larger energy barrier of 68 meV and according to ^{13}C MAS NMR effectively restore the high molecular site symmetry (Fig. 4b) above 195 K. A crossover from the dynamic to the static regime appears on the NMR time-scale between 195 and 120 K before finally static JT deformations of C_{60}^{3-} ions are seen on the NMR time-scale below ~120 K. While IR measurements have set a lower limit for the interconversion correlation time of the JT conformers at ~10^{-11} s,[11] the present low-temperature MAS NMR experiments now define an upper limit of ~10^{-5} s. However, ^{133}Cs MAS NMR tells us at the same time that the C_{60}^{3-} merohedral disorder remains unaffected by the variations in the JT conformer arrangements. Therefore, the JT effect must be local and the interactions between JT deformations on neighboring molecules, which could lead to the cooperative JT effect at low temperatures, are weak compared to the variation of the JT energies imposed by the C_{60}^{3-} merohedral disorder. Because the whole process is driven by the merohedral disorder, the global

structural and electronic cubic symmetry is preserved and JT deformations freeze-in in a random fashion with no or weak orbital correlations producing an orbital glass state (Fig. 4c). This glassy electronic state also provides a natural explanation for the observed severe magnetic spatial disorder and inhomogeneity, which accompany spin freezing in the magnetically frustrated fcc topology of Cs_3C_{60} below ~2.2 K.[4]

Conclusions

In conclusion, it appears that in the insulating Cs_3C_{60}, the Jahn-Teller effect is strong enough to overcome Hund's rule to enforce a low-spin state,[3–5] but at the same time it is not strong enough to break the global cubic symmetry, notwithstanding the merohedral disorder. The present results for Cs_3C_{60} thus demonstrate the active role of the JT effect in the Mott-Jahn-Teller-insulating phase[53] and suggest the interplay between lattice, orbital, spin, and charge degrees of freedom in the vicinity of the insulator-to-metal instability in these strongly-correlated molecular systems. The Jahn-Teller effect is not dynamic at all temperatures and thus a unique orbital-glass highly-disordered antiferromagnetic Mott-Jahn-Teller-insulating state emerges at low temperatures due to the coupling to the local structural distortions.

Therefore, the resulting molecular symmetries in the high temperature superconducting states accessed upon the application of pressure should be carefully considered in future studies, since the merohedral disorder does not change across the insulator-metal/superconductor boundary. The simplest picture is that the local structure in merohedral fcc metallic A_3C_{60} will be the same as the average one because in the metal the t_{1u} electrons are delocalized and thus the local JT effect is suppressed. However, there are many other possible scenarios – the work here shows that the NMR timescale is needed to distinguish static and dynamic JT effects and that even in a material cubic to diffraction, the local symmetry of individual C_{60}^{3-} anions is lower than consistent with cubic local symmetry.

Acknowledgements

We acknowledge financial support by the European Union FP7-NMP-2011-EU-Japan project LEMSUPER (Contract No. NMP3-SL-2011-283214), the Slovenian Research Agency (Project No. J1-2284), the Estonian Research Agency (ETF8198, SF0690034s09), and the Engineering and Physical Sciences Research Council, UK (Grant No. EP/K027255 and EP/K027212). D.A. thanks Durham University for the award of a Senior Research Fellowship and K.P. the Royal Society for a Wolfson Research Merit Award. M.J.R. is a Royal Society Research Professor.

Notes and references

[a] Jožef Stefan Institute, Jamova cesta 39, 1000 Ljubljana, Slovenia.
[b] Department of Chemistry, University of Liverpool, Liverpool L69 7ZD, UK.
[c] Department of Chemistry, Durham University, Durham DH1 3LE, UK.
[d] National Institute of Chemical Physics and Biophysics, Akadeemia tee 23, 12618 Tallinn, Estonia.
[e] EN-FIST Centre of Excellence, Dunajska cesta 156, 1000 Ljubljana, Slovenia.
[f] WPI Research Center, Advanced Institute for Materials Research, Tohoku University, Sendai 980-8577, Japan.
[g] Faculty of mathematics and physics, University of Ljubljana, Jadranska cesta 19, 1000 Ljubljana, Slovenia.

Electronic Supplementary Information (ESI) available: [high-temperature static ^{133}Cs NMR spectra proving frozen-in merohedral disorder (Fig. S1); extracted parameters of the ^{133}Cs and ^{13}C MAS NMR peaks (Table S1) and the predicted intensities for the ^{133}Cs NMR O-peaks (Table S2); fits of the ^{133}Cs MAS NMR spectra (Fig. S2) allowing us to extract temperature dependences of NMR linewidths (Fig. S3); Clogston-Jaccarino plots for ^{133}Cs MAS NMR peaks (Fig. S4).]. See DOI: 10.1039/b000000x/

1. (a) O. Gunnarsson, *Alkali-doped fullerides*, World Scientific, Singapore, 2004; (b) M. J. Rosseinsky, *Chem. Mater*., 1998, **10**, 2665–2685; (c) S. Margadonna and K. Prassides, *J. Solid State Chem*., **168**, 639–652 (2002).
2. A. Y. Ganin, Y. Takabayashi, Y. Z. Khimyak, S. Margadonna, A. Tamai, M. J. Rosseinsky, and K. Prassides, *Nat. Mater.*, 2008, **7**, 367–371.
3. Y. Takabayashi, A. Y. Ganin, P. Jeglič, D. Arčon, T. Takano, Y. Iwasa, Y. Ohishi, M. Takata, N. Takeshita, K. Prassides, and M. J. Rosseinsky, *Science*, 2009, **323**, 1585–1590.
4. A. Y. Ganin, Y. Takabayashi, P. Jeglič, D. Arčon, A. Potočnik, P. J. Baker, Y. Ohishi, M. T. McDonald, M. D. Tzirakis, A. McLennan, G. R. Darling, M. Takata, M. J. Rosseinsky, and K. Prassides, *Nature*, 2010, **466**, 221–225.
5. P. Jeglič, D. Arčon, A. Potočnik, A. Y. Ganin, Y. Takabayashi, M. J. Rosseinsky, and K. Prassides, *Phys. Rev. B*, 2009, **80**, 195424–195428.
6. G. R. Darling, A. Y. Ganin, M. J. Rosseinsky, Y. Takabayashi, and K. Prassides, *Phys. Rev. Lett.*, 2008, **101**, 136404–136407.
7. S. Chakravarty, M. P. Gelfand, and S. Kivelson, *Science*, 1991, **254**, 970–974.
8. M. Capone, M. Fabrizio, C. Castellani, and E. Tosatti, *Rev. Mod. Phys.*, 2009, **81**, 943–958.
9. Y. Murakami, P. Werner, N. Tsuji, and H. Aoki, *Phys. Rev. B*, 2013, **88**, 125126–125139.
10. C. C. Chancey and M. C. M. O'Brien, *The Jahn-Teller Effect in C_{60} and Other Icosahedral Complexes*, Princeton University Press, 1997.
11. G. Klupp, P. Matus, K. Kamarás, A. Y. Ganin, A. McLennan, M. J. Rosseinsky, Y. Takabayashi, M. T. McDonald, and K. Prassides, *Nat. Commun.*, 2012, **3**, 912–917.
12. O. Gunnarsson, J. E. Han, E. Koch, and V. H. Crespi, in *Superconductivity in Complex Systems*, eds. K. A. Müller and A. Bussmann-Holder, Springer Berlin Heidelberg, 2005, pp. 71–101.
13. N. Iwahara and L. F. Chibotaru, *Phys. Rev. Lett.*, 2013, **111**, 056401.
14. A. Potočnik, N. Manini, M. Komelj, E. Tosatti, and D. Arčon, *Phys. Rev. B*, 2012, **86**, 085109.

15. R. Blinc, P. Jeglič, T. Apih, J. Seliger, D. Arčon, and A. Omerzu, *Phys. Rev. Lett.*, 2002, **88**, 86402.
16. P. Jeglič, R. Blinc, T. Apih, A. Omerzu, and D. Arčon, *Phys. Rev. B*, 2003, **68**, 184422.
17. K. Prassides, S. Margadonna, D. Arčon, A. Lappas, H. Shimoda, and Y. Iwasa, *J. Am. Chem. Soc.*, 1999, **121**, 11227–11228.
18. S. Margadonna, K. Prassides, H. Shimoda, T. Takenobu, and Y. Iwasa, *Phys. Rev. B*, 2001, **64**, 132414.
19. A. Y. Ganin, Y. Takabayashi, C. A. Bridges, Y. Z. Khimyak, S. Margadonna, K. Prassides, and M. J. Rosseinsky, *J. Am. Chem. Soc.*, 2006, **128**, 14784–14785.
20. A. Y. Ganin, Y. Takabayashi, M. Pregelj, A. Zorko, D. Arc□on, M. J. Rosseinsky, and K. Prassides, *Chem. Mater.*, 2007, **19**, 3177–3182.
21. D. Arčon, M. Pregelj, A. Zorko, A. Y. Ganin, M. J. Rosseinsky, Y. Takabayashi, K. Prassides, H. van Tol, and L. C. Brunel, *Phys. Rev. B*, 2008, **77**, 035104.
22. D. Arc□on, A. Y. Ganin, Y. Takabayashi, M. J. Rosseinsky, and K. Prassides, *Chem. Mater.*, 2008, **20**, 4391–4397.
23. G. Zimmer, M. Mehring, C. Goze, and F. Rachdi, *Phys. Rev. B*, 1995, **52**, 13300–13305.
24. G. Klupp, K. Kamarás, N. M. Nemes, C. M. Brown, and J. Leao, *Phys. Rev. B*, 2006, **73**, 085415.
25. P. W. Stephens, L. Mihaly, P. L. Lee, R. L. Whetten, S.-M. Huang, R. Kaner, F. Deiderich, and K. Holczer, *Nature*, 1991, **351**, 632–634.
26. R. E. Walstedt, D. W. Murphy, and M. Rosseinsky, *Nature*, 1993, **362**, 611–613.
27. H. Alloul, K. Holczer, Y. Yoshinari, and O. Klein, *Phys. C Supercond.*, 1994, **235–240**, 2509–2510.
28. Y. Yoshinari, H. Alloul, K. Holczer, and L. Forro, *Phys. C Supercond.*, 1994, **235–240**, 2479–2480.
29. Y. Yoshinari, H. Alloul, V. Brouet, G. Kriza, K. Holczer, and L. Forro, *Phys. Rev. B*, 1996, **54**, 6155.
30. M. Kraus, O. Klein, G. Buntkowsky, and K. Lüders, *Phys. B Condens. Matter*, 1999, **271**, 7–14.
31. G. Zimmer, K. F. Thier, M. Mehring, F. Rachdi, and J. E. Fischer, *Phys. Rev. B*, 1996, **53**, 5620.
32. G. Zimmer, M. Helmle, M. Mehring, F. Rachdi, J. Reichenbach, L. Firlej, and P. Bernier, *EPL Europhys. Lett.*, 1993, **24**, 59.
33. A. Samoson, T. Tuherm, J. Past, A. Reinhold, T. Anupõld, and I. Heinmaa, in *New Techniques in Solid-State NMR*, ed. J. Klinowski, Springer Berlin Heidelberg, 2005, pp. 15–31.
34. K. R. Thurber and R. Tycko, *J. Magn. Reson.*, 2008, **195**, 179–186.
35. R. Sarkar, M. Concistrè, O. G. Johannessen, P. Beckett, M. Denning, M. Carravetta, M. al-Mosawi, C. Beduz, Y. Yang, and M. H. Levitt, *J. Magn. Reson.*, 2011, **212**, 460–463.
36. P. Beckett, M. S. Denning, I. Heinmaa, M. C. Dimri, E. A. Young, R. Stern, and M. Carravetta, *J. Chem. Phys.*, 2012, **137**, 114201–114201–5.
37. P. Beckett, M. S. Denning, M. Carravetta, A. Kalda, and I. Heinmaa, *J. Magn. Reson.*, 2012, **223**, 61–63.
38. See supplementary information.
39. Y. Maniwa, T. Saito, A. Ohi, K. Mizoguchi, K. Kume, K. Kikuchi, I. Ikemoto, S. Suzuki, Y. Achiba, M. Kosaka, K. Tanigaki, and T. W. Ebbesen, *J. Phys. Soc. Jpn.*, 1994, **63**, 1139–1148.
40. N. Sato, H. Tou, Y. Maniwa, K. Kikuchi, S. Suzuki, Y. Achiba, M. Kosaka, and K. Tanigaki, *Phys. Rev. B*, 1998, **58**, 12433.
41. C. H. Pennington and V. A. Stenger, *Rev. Mod. Phys.*, 1996, **68**, 855.
42. A. Auerbach, N. Manini, and E. Tosatti, *Phys. Rev. B*, 1994, **49**, 12998–13007.
43. M. J. Duer, *Solid State NMR Spectroscopy: Principles and Applications*, Wiley, 2002.
44. Y. Ihara, H. Alloul, P. Wzietek, D. Pontiroli, M. Mazzani, and M. Riccó, *Phys. Rev. Lett.*, 2010, **104**, 256402.
45. Y. Ihara, H. Alloul, P. Wzietek, D. Pontiroli, M. Mazzani, and M. Riccò, *EPL Europhys. Lett.*, 2011, **94**, 37007.
46. P. Wzietek, T. Mito, H. Alloul, D. Pontiroli, M. Aramini, and M. Riccò, *Phys. Rev. Lett.*, 2014, **112**, 066401.
47. A. Potočnik, A. Krajnc, P. Jeglič, Y. Takabayashi, A. Y. Ganin, K. Prassides, M. J. Rosseinsky, and D. Arčon, *Sci. Rep.*, 2014, **4**, 4265.
48. V. Brouet, H. Alloul, F. Quéré, G. Baumgartner, and L. Forró, *Phys. Rev. Lett.*, 1999, **82**, 2131–2134.
49. S. Satpathy, V. P. Antropov, O. K. Andersen, O. Jepsen, O. Gunnarsson, and A. I. Liechtenstein, *Phys. Rev. B*, 1992, **46**, 1773–1793.
50. A. Abragam, *The principles of nuclear magnetism*, Clarendon Press□; Oxford University Press, Oxford [Oxfordshire]; New York, 1983.
51. H. Keller and A. Bussmann-Holder, *Adv. Condens. Matter Phys.*, 2010, **2010**, 393526.
52. H. Keller, A. Bussmann-Holder, and K. A. Müller, *Mater. Today*, 2008, **11**, 38–46.
53. M. Fabrizio and E. Tosatti, *Phys. Rev. B*, 1997, **55**, 13465–13472.

